Insights on the role of Ru substitution in the properties of $LaCoO_3$-based oxides as catalysts precursors for the oxidative reforming of diesel fuel

N. Mota[a], M.C. Alvarez-Galván[a], R.M. Navarro[a], J.L.G. Fierro[a],

S.M. Al-Zahrani[b], A. Goguet[c], H. Daly[c], W. Zhang[d], A. Trunschke[d], R. Schlögl[d]

[a]Instituto de Catálisis y Petroleoquímica (CSIC), Marie Curie 2, Cantoblanco 28049, Madrid, Spain; [b]Chemical Engineering Department, College of Engineering, King Saud University, Riyadh, Kingdom of Saudi Arabia; [c]CenTACat, School of Chemistry and Chemical Engineering, Queen's University Belfast, Belfast BT9 5AG, Northern Ireland, United Kingdom; [d]Fritz-Haber-Institute of the Max-Planck-Society, Department of Inorganic Chemistry, Faradayweg 4-6, 14195 Berlin, Germany

Abstract

The partial substitution of Co by Ru in lanthanum cobaltite perovskites ($LaCo_{1-x}Ru_xO_3$, x = 0.05 and 0.2) and its influence on the reducibility and structural modifications in the perovskite lattice have been evaluated by N_2 adsorption isotherms, in-situ XRD, TPR and XPS. Characterization of $LaCo_{1-x}Ru_xO_3$ perovskite precursors reveal that Ru is incorporated into the perovskite lattice, producing a distortion of the original rhombohedral structure, a decrease in mean crystallite size and some increase in the surface area. The structural evolution of the $LaCo_{1-x}Ru_xO_3$ precursors under a reductive treatment indicates that Ru promotes the reducibility of the perovskite leading to a greater reduction degree of cobalt species. Moreover, the smaller perovskite crystallites obtained with the partial substitution of cobalt by ruthenium evolve to smaller crystal domains of both Co^0 and La_2O_3 after reduction. The catalysts formed after the reduction of perovskite precursors present very high catalytic efficiency to extract hydrogen from diesel molecules by oxidative reforming. However, those catalysts derived from Ru-substituted perovskites show better catalytic performance associated to the higher development of active metallic phases achieved on the surface of these catalysts. Additionally, Ru promotes the catalytic activity and stability for this reaction increasing the reduction degree of cobalt and decreasing coke formation and sulfur poisoning through the formation of smaller cobalt crystallites.

Keywords: hydrogen, diesel, oxidative reforming, lanthanum cobaltite, ruthenium

1. Introduction

There is an increasing interest in the development of technologies for the conversion of hydrocarbons in hydrogen rich gas mixtures as a way to overcome the current technical limitations in hydrogen supply and storage. Among the different logistic fuels, diesel fuel is an excellent candidate to produce hydrogen by reforming due to its low price, high volumetric and gravimetric energy density, availability and well established supply infrastructure. However, its reforming is difficult due to the harsh operating conditions such as high reaction temperature, coke formation and sulphur poisoning [1~~1~~]. Conventional and low price nickel-based catalysts, widely used for hydrogen production, are not stable for this purpose, since coke is formed in large amounts [2~~2~~] and they do not tolerate sulfur compounds [3~~3~~]. Thus, the successful extraction of hydrogen from diesel molecules largely depends on the development of catalysts with high thermal stability and improved properties with respect to coke formation and sulphur poisoning. For higher hydrocarbon reforming, the catalyst typically comprises metals such as Pt, Rh or Ru deposited or incorporated into carefully engineered oxide supports promoted or doped with elements for improved thermal stability or better activity [4~~4~~]. With the non-noble metal formulations, such as Fe, Co or Ni supported on ion-conducting doped ceria-substrates, activities similar to PGM-containing catalysts has been reported [4~~4~~]. In the search for new catalysts with improved activity for diesel reforming, the use of perovskite type oxides, ABO_3, as catalyst precursors is a good alternative due to the possibility to form, by reduction, finely dispersed active metal particles of B atoms supported on a highly stable oxide of A. The key feature that make these oxides suitable as catalyst precursors are that, under reductive reaction conditions, the active phase is segregated out as small and well dispersed particles, which increases hydrogen formation and prevents deactivation by coke and sulfur [1~~1~~,5~~5~~]. $LaCoO_3$ is particularly attractive, because it is one of the most reducible ABO_3-type perovskites and it forms after reduction highly dispersed Co particles in close contact with La_2O_3 which have been reported to have a role in improving catalyst stability favouring coke gasification [6~~6~~]. A way to achieve more active and stable catalysts for heavy hydrocarbon reforming and tailor the catalytic properties is by producing structural and electronic modifications by partial substitution of Co sites by another cation in the perovskite lattice of the precursor [7~~7~~,8~~8~~]. Among transition metals substituting Co in the perovskite lattice, ruthenium was particularly effective in catalytic reforming of heavy hydrocarbon fuels. In previous papers, we have shown that the introduction of Ru in the catalyst derived from $LaCoO_3$ increases the efficiency in the catalytic reforming of heavy hydrocarbon fuels, producing higher hydrogen yields

Formatiert: Schriftart: (Standard)
Formatiert: Schriftart: (Standard)
Formatiert: Schriftart: (Standard)
Formatiert: Schriftart: (Standard)
Formatiert: Schriftart: (Standard)
Formatiert: Schriftart: (Standard)
Formatiert: Schriftart: (Standard)
Formatiert: Schriftart: (Standard)
Formatiert: Schriftart: (Standard)

and more stable systems [99,1010]. Discarding the intrinsic activity of ruthenium, this improved catalytic behavior is attributed to structural changes produced in the perovskite lattice that manifest a higher exposition of active phases formed during reaction.

With this background, the objective of this work is to gain insight about the influence of the partial substitution of Co by Ru over the physicochemical properties of $LaCo_{1-x}Ru_xO_3$ perovskite precursors. The influence of the ruthenium substitution degree in the $LaCo_{1-x}Ru_xO_3$ perovskite precursor (x= 0.05 or 0.2) on the reducibility of the perovskite and its effect over the surface composition and structure of derived catalysts has been studied. The correlation of activity performance with catalysts characterization results, in fresh and used state, allows us to gain knowledge on the effect of the ruthenium substitution in perovskite precursors over the physicochemical characteristics and the activity and stability of the derived catalysts.

2. Experimental

2.1 Perovskites preparation

Perovskite precursors were synthesized by a modified citrate sol-gel method [1111]. 1 M aqueous nitrate solutions containing the precursor cations ($La(NO_3)_3 \cdot 6H_2O$ (99.9%), $Co(NO_3)_2 \cdot 6H_2O$ (97.7%) and $RuCl_3$ (40.49% Ru), all from Johnson Matthey, were added to a solution of citric acid (Johnson Matthey) and ethylene glycol (Riedel-de Haën) (molar ratio 1:1 and citric acid/(La+(Co+Ru))= 2.5). The mixture was stirred and heated at 343 K for 5 h in order to evaporate the excess of solvent and promote polymerization. After some hours, a black or purple, highly viscous gel was obtained for mixtures with or without Ru, respectively. The obtained product was charred at 573 K for 2 h to remove the organic matter and calcined under air at 1023 K for 4 h.

2.2 Physicochemical characterization

The specific BET area of the perovskite precursors and catalysts was calculated from the nitrogen adsorption-desorption isotherms at 77 K, recorded with a Micromeritics ASAP 2100 apparatus. Prior to adsorption the samples were degassed at 423 K under vacuum ($P < 3 \times 10^{-5}$ mbar) for 4 h.

XRD of perovskite precursors and fresh and used catalysts were recorded using a Seifert 3000P vertical diffractometer and nickel-filtered Cu Kα radiation (λ = 0.1538 nm)

Formatiert: Schriftart: (Standard)
Formatiert: Schriftart: (Standard)
Formatiert: Schriftart: (Standard) Arial, Englisch (USA)
Feldfunktion geändert

under constant instrumental parameters. For each sample, Bragg angles between 5º and 80º were scanned; a rate of 5 s per step (step size: 0.04º) was used during a continuous scan in the above-mentioned range. The mean $LaCoO_3$ particle size was then estimated from X-ray line width broadening using the Scherrer equation. Width (t) was taken as the full width at half maximum intensity of the most intense and least overlapped peak (2θ = 47.5º).

In-situ X-ray diffraction (XRD) patterns during the reduction of perovskite precursors were obtained on a PANalytical X-ray diffractometer using Ni-filtered Cu Kα radiation. XRD profiles during the reduction of perovskite precursors were measured at different temperatures (room temperature, 373, 473, 573, 673, 773, 873, 973 and 973 K after 1 h) by scanning steps (step size, 0.0167º) in the 2θ ranges between 20 and 50º, with a ramp of 10 K/min, under flowing 10% H_2/N_2 (mol %, 50 mlN/min).

Hydrogen temperature-programmed reductions (H_2-TPR) were conducted using a Micromeritics 2900 instrument by heating the sample under a 10% H_2/Ar flow (50 mL/min) up to 973 K at a linearly programmed rate of 10 K/min.

A Philips CM200-FEG transmission electron microscope operated at 200 kV (point resolution, 0.19 nm) was employed to conduct high resolution transmission electron microscopy (HR-TEM) analyses of the fresh catalysts. The TEM was equipped with the EDAX Genesis detector. The perovskite precursors were reduced under the same conditions used in the activation pretreatment, before reaction, with a reductive stream of 50 mL/min (10% H_2/N_2) at 973 K for 1 h. The reduced samples were transferred from the glove box to the TEM by a vacuum holder, without exposure to air.

X-ray photoelectron spectra were recorded using an Escalab 200R spectrometer equipped with a hemispherical electron analyzer and an Al Kα ($h\nu$ = 1486.6 eV, 1 eV = 1.6302 x 10^{-19} J) 120 W X-ray source. Charging effects were corrected by referencing the binding energies (BE) to the C 1s signal at 284.6 eV arising from carbon contamination. The area of the peaks was estimated by calculating the integral of each peak after smoothing and subtraction of an S-shaped background and fitting of the experimental curve to a mixture of Lorentzian and Gaussian lines of variable proportions. Quantification of the atomic fractions on the sample surface was obtained by integration of the peaks with appropriate corrections for sensitivity factors [12~~12~~].

Elemental Chemical Analysis was performed to determine the carbon and sulfur content in the used catalysts. This was accomplished using a Leco CHNS-932 device with an AD-4 Perkin-Elmer autobalance.

Feldfunktion geändert

Formatiert: Schriftart: (Standard) Arial, Englisch (USA)

2.3 Activity tests

Diesel reforming tests were performed in a fixed-bed reactor at atmospheric pressure and a reaction temperature of 1023 K, to avoid maximum conversion and be able to discriminate among the different catalysts. The catalytic bed, 100 mg of perovskite precursor, was placed in a tubular reactor (8-mm i.d) with a coaxially centred thermocouple in contact with the catalytic bed. Before the catalytic tests, the precursors were activated by reduction under a 10% H_2/N_2 flow (50 mlN/min, T = 973 K, 1 h). Reactants were fed at a molar ratio of $H_2O/O_2/C$ = 3/0.5/1. To decrease coke formation, a high H_2O/C ratio was used. Diesel and water were separately introduced by using two HPLC pumps and vaporized in a preheater (473 K) before being passed through the catalyst bed. The gas flow rate was kept at 75 mlN/min (GHSV=20000 h^{-1}). The products were analysed periodically with on-line gas chromatograph (HP 5890 Series II) equipped with a TC detector which was programmed to operate under high sensitivity conditions (4A-molecular sieve column for H_2, O_2, N_2, CO and CH_4 separation and Porapack N (80/100) for CO_2, C_2H_4, C_2H_6 and H_2O). Water (steam) and heavy hydrocarbons were condensed in a condensate trap before reaching the gas chromatograph.

Activity data were reported as diesel conversion, hydrogen yield (moles of hydrogen and CO produced by carbon atom in the feed, considering also the hydrogen that will be produced by the subsequent WGS reaction stage (with an ideal efficiency equal to 1)) and selectivities to the different products. These diesel conversion, hydrogen yield and selectivity of products are defined as follows:

Diesel conversion (%): $$\frac{(\text{mole } C_mH_n)_{in} - (\text{mole } C_mH_n)_{out}}{(\text{mole } C_mH_n)_{in}} \times 100 \quad (1)$$

Hydrogen yield: $$\frac{(\text{mole amount of } H_2 + CO)_{out}}{(\text{total mole amount C})_{in}} \quad (2)$$

Product distribution: (%) (i: H_2, CO, CH_4, CO_2, C_2H_4, C_2H_6, C_3H_6):

$$\frac{(\text{mole i})_{out}}{\sum mole\ i_{out}} \times 100 \quad (3)$$

3. Results

3.1 Characterization of perovskite precursors

XRD patterns of perovskite precursors (Fig. 1) show in all cases the presence of a well-defined perovskite structure with high degree of crystallinity and homogeneity (JCPDS 048-0848). For Ru-containing samples, the typical doublet characteristic of the rhombohedral structure disappears, this effect being more pronounced with increasing Ru substitution (Fig. 2). For these samples, a distortion of the rhombohedral phase is produced (JCPDS 01-086-1665). In addition, all the samples display a small peak around 44.5º whose origin lies in the presence of a small fraction of segregated cubic Co_3O_4 phase with a preferential growth of (400) plane. No diffraction lines could be attributed to specific Ru-containing particles. It is also observed (Fig. 2) that the partial substitution of Co by Ru shifts the diffraction lines toward lower angle values. This shift suggests that the Ru cation incorporates at the B position of the perovskite lattice [10~~10~~], more likely as Ru^{4+}, favoured under the oxidation conditions used in the final calcination step~~,~~ during the syntheses of these samples [13~~13~~-15~~15~~]. For the Ru-loaded samples, the observed X-ray line broadening points to a decrease in the crystallite domains. To quantify this effect, average grain sizes were calculated using the Scherrer equation. The results (shown in Table 1) reveal a decrease in the mean crystallite size of the perovskite with the partial substitution of Co by Ru in the perovskite lattice, this drop being more pronounced for the $LaCoRu_{0.2}$ sample.

BET surface areas of $LaCo_{1-x}Ru_xO_3$ precursors calculated from N_2 adsorption-desorption isotherms are also included in Table 1. As observed in this table, all precursors displayed low values of surface area supporting the fact that perovskite precursors did not develop a nanoporous structure. It is also found that the surface area of the perovskite precursors varied with the incorporation of Ru into the perovskite lattice, with some increase in surface area in Ru-containing samples observed. A similar trend has been also observed for $LaRu_{1-x}Ni_xO_3$, for substitutions between x = 0.2-0.6 [16~~16~~].

Structural evolution of perovskite precursors during reduction was studied by in-situ XRD and the diffraction patterns obtained during the reduction of the different perovskites, shown in Fig. 3, nicely illustrate the temperatures at which phase changes

Formatiert: Schriftart: (Standard) Arial, Englisch (USA)

Feldfunktion geändert

Formatiert: Schriftart: (Standard) Arial, Englisch (USA)

Formatiert: Schriftart: (Standard) Arial, Englisch (USA)

Feldfunktion geändert

Feldfunktion geändert

Formatiert: Schriftart: (Standard) Arial, Englisch (USA)

Feldfunktion geändert

occur. For all the precursors, it can be observed that an increase in the temperature up to 473 K under a reductive atmosphere produces a shift of the main diffraction lines to lower diffraction angles, a consequence of the thermal expansion of the perovskite lattice. For bare $LaCoO_3$, the formation of a new structure that could be attributed to a brownmillerite phase ($La_3Co_3O_8$) formed by the partial reduction of Co ions is observed at 573 K [17]. The structural evolution of the precursor continues with the increase in the reduction temperature, observing in the range 673-773 K the appearance of phases formed by the partial reduction of Co ions corresponding to La_2CoO_4 (JCPDS 034-1081) (main diffraction line at 31.4º) and phases from Ruddlesden-Popper series ($La_{m+1}Co_mO_{3m+1}$) such as $La_4Co_3O_{10}$ (JCPDS 034-1150, 32.5º) [18~~18~~]. At 873 K, the XRD pattern of the $LaCoO_3$ precursor shows the complete reduction of Co ions with the formation of hexagonal La_2O_3 (JCPDS 083-1344) and cubic metallic cobalt (JCPDS 015-0806) crystallites (Fig. 3). The intensity and narrowness of these phases increase with a further increase in reduction temperature indicative of the crystalline growth of metallic Co and La_2O_3 phases. On the other hand, an increase in the temperature from 298 to 673 K produces a progressive decrease of the diffraction line corresponding to cobalt oxide spinel, until it disappears, due to the reduction of this phase.

For the Ru-loaded samples, an increase in temperature to 473 K, also gives a shift of the diffraction peaks to lower diffraction angles but does not produce significant changes in the perovskite structure. The reduction of cobalt starts at lower temperature as observed with the formation of phases with Co^{2+} at 773 K, such as La_2CoO_4 and $La_4Co_3O_{10}$. For Ru-containing samples, a decrease of the diffraction peak associated to Co_3O_4 until its disappearance at 773 K is also noted. The complete reduction of Co phases for the Ru-containing precursors is observed at a temperature much lower than that found for the bare lanthanum cobaltite. Thus for Ru-containing samples, the formation of hexagonal La_2O_3 (JCPDS 083-1344) and cubic metallic cobalt (JCPDS 015-0806) crystallites are observed at reduction temperatures of around 773 K. For Ru-containing samples, it should be pointed out the coexistence of cubic (JCPDS 022-0369) and hexagonal lanthana at 773 and 873 K. For higher reduction temperatures, only the presence of hexagonal crystallites of La_2O_3 which are growing together with Co^0 crystallites are observed.

No diffraction lines corresponding to ruthenium species were observed in any of the above XRD patterns. As will be derived from HRTEM analyses of reduced samples, the reduction produces the formation of Ru^0 particles, although with crystalline domains too small to be detected by XRD.

Feldfunktion geändert

Feldfunktion geändert

Formatiert: Schriftart: (Standard) Arial, Englisch (USA)

The TPR profiles for the $LaCo_{1-x}Ru_xO_3$ perovskite series are displayed in Fig. 4. The TPR experiments show two main reduction peaks: a first contribution with maxima at 540–645 K, and a second at 805-845 K for all the samples. In accordance with the structural evolution of precursors during the reduction observed by in-situ XRD (Figure 3), the first main peak is attributed to the reduction of Co (III) to Co (II) and the second to the reduction of Co(II) to metallic cobalt [~~19~~19,~~20~~20]. ~~$LaCoO_3$ and $LaCo_{0.95}Ru_{0.05}O_3$~~ samples show an overlapping peak in the first hydrogen consumption that includes the reduction of the perovskite structure to $LaCoO_{2.67}$ ($La_3Co_3O_8$ phase that it is then decomposed in La_2CoO_4 and CoO) [~~17~~] and the reduction of segregated cobalt oxide spinel particles, already observed by XRD [~~11~~].

Looking at the reduction temperatures, there is a marked effect of Ru in the reducibility of $LaCoO_3$ phase, in accordance also with results obtained by in-situ XRD, where a shift of the first reduction peak to lower temperatures with the partial substitution of Co by Ru in the perovskite lattice was observed. Although the position of reduction peaks also depends on the type of structure, crystallite size and oxygen defects of perovskites [~~10~~10,~~21~~21,~~22~~22], which are modified with the addition of Ru, the incorporation of noble metals also enhances the reducibility of cobalt ions via hydrogen spillover [~~11~~11,~~10~~10,22,~~23~~23]. Therefore, Ru metal formed by the reduction of surface ruthenium phase would favour the reduction of cobalt by H-spillover in this first reduction step.

3.2 Bulk and surface structures of catalysts

As indicated in the experimental section, the perovskite precursors were transformed in catalysts by reduction before reaction. XRD patterns corresponding to samples treated at 973 K (figure 3) show a complete restructuring of initial perovskite precursors into a mixture of hexagonal lanthanum oxide and cubic metallic cobalt particles (figure 3). None of the fresh reduced catalysts exhibited any reflection corresponding to metallic ruthenium. This could be indicative of a high dispersion of metallic ruthenium forming crystallites with a size lower than 4 nm undetectable by this technique. Quantitative estimation of crystalline domains of Co^0 and La_2O_3 in fresh catalysts, by applying the Scherrer equation (Table 2), indicates a decrease of Co^0 and La_2O_3 crystalline domains with the increase in the partial substitution of cobalt by ruthenium in the perovskite precursor.

The morphology and structure of the reduced catalysts were investigated by HRTEM. The images have been recorded on samples derived from a reduction treatment of perovskites $LaCoO_3$ and $LaCo_{0.8}Ru_{0.2}O_3$, already described in the experimental section, reproducing the pretreatment conditions followed in the reaction system. Figure 5

Formatiert: Schriftart: (Standard) Arial, Englisch (USA)
Feldfunktion geändert
Formatiert: Schriftart: (Standard)
Feldfunktion geändert
Feldfunktion geändert
Feldfunktion geändert
Formatiert: Schriftart: (Standard) Arial, Englisch (USA)
Formatiert: Schriftart: (Standard) Arial, Englisch (USA)
Formatiert: Schriftart: (Standard) Arial, Englisch (USA)
Formatiert: Schriftart: (Standard) Arial, Englisch (USA)
Formatiert: Schriftart: (Standard) Arial, Englisch (USA)
Formatiert: Schriftart: (Standard) Arial, Englisch (USA)
Formatiert: Schriftart: (Standard) Arial, Englisch (USA)

shows typical HRTEM micrographs of the catalyst derived from reduction of bare $LaCoO_3$, being observed quasi-spherical *fcc* Co^0 nanoparticles with a diameter around 5-25 nm. The lattice fringes (1 1 1) of metallic cobalt were identified with their acute angle [24~~24~~,25~~25~~], which is in accordance with the phase found by XRD. Moreover, one can find many stacking faults and micro-twinning of typical metallic cobalt, as indicated by the arrows. The HRTEM micrographs of the catalyst derived from the reduction of $LaCo_{0.8}Ru_{0.2}O_3$ precursor are shown in Figure 6. Together with *fcc* metallic cobalt particles, small nanoparticles of Ru (some of them smaller than 5 nm) in its metallic phase were found, based on measurements of the lattices fringes of the (1 0 1) and (0 1 1) crystal planes with their characteristic acute angle.

The chemical composition of above reduced samples was determined by STEM/EDX elemental mapping, as shown in Fig. 7. One can find that the constituting elements are homogenously distributed in the sample at this low magnification scale. On the other hand, the EDX analyses (Table 3), performed on a large area, give an average Co/La and Ru/Co/La ratios close to the nominal ones.

XPS analyses were performed to probe the surface chemical composition of the reduced catalysts. The binding energies of core-levels of all the fresh reduced samples (Fig. 8) indicate that both metallic cobalt (~ 778 eV) and cobalt oxide (~ 780 eV) [26] are present on the catalyst surface. The Co 2p line profile of the catalyst derived from $LaCoO_3$ displays a satellite line somewhere around 790 eV which is the fingerprint of Co_3O_4 species. On the contrary, the catalyst derived from $LaCo_{0.95}Ru_{0.05}O_3$ shows this satellite peak placed at 786 eV which is characteristic of CoO [26~~26~~]. For the reduced $LaCo_{0.8}Ru_{0.2}O_3$ sample these satellites, associated to the presence of cobalt oxide on the surface, almost disappear, indicating the fact that cobalt phase is mostly in the metallic state. The greater reduction degree of cobalt phase by the presence of ruthenium has been also reported and discussed on the basis of results obtained by TPD of CO and CO_2 and by TPSR of propane [27~~27~~].

The binding energy values of La $3d_{5/2}$ core-level spectra of reduced samples also point to a greater degree of reduction upon increasing the substitution of Co by Ru. Thus, the La 3d level corresponding to Ru-containing catalysts shows a more resolved profile with binding energies around 835 eV indicative of the presence of La^{3+} ions in a higher purity lanthana phase [28], mostly carbonated and/or hydroxylated [29,30]. Thus, surface lanthana can strongly adsorb CO_2, already existing at the surface of the perovskite precursor, and also hydroxyl groups, produced during the formation of water in the reduction process [31].

Formatiert: Schriftart: (Standard) Arial, Englisch (USA)

Formatiert: Schriftart: (Standard)

Formatiert: Schriftart: (Standard) Arial, Englisch (USA)

Formatiert: Schriftart: (Standard) Arial, Englisch (USA)

In parallel with the appearance of the La_2O_3 phase, Ru^0 phase is expected to appear. This was confirmed by the binding energy of the $Ru3p_{3/2}$ level whose binding energy appears close to 462 eV, typical of metallic ruthenium [11].

Atomic surface ratios have been calculated and the respective values are compiled in Table 4. The most significant is the higher surface exposition of La phase in relation to the element in the B position (Co or Ru), considering the nominal ratio (=1). It should also be pointed out that there is a greater relative surface proportion of elements in the B position for the samples with Ru. In the case of the catalyst derived from the $LaCo_{0.8}Ru_{0.2}O_3$ precursor, the low relative surface proportion of cobalt is compensated by the high value for Ru. On the other hand, the high proportion of non-lattice oxygen in these fresh reduced catalysts with Ru should be noted, being higher for the sample derived from the more substituted lanthanum cobaltite. This result is explained by the greater surface proportion of lanthana, derived from the higher reduction degree of $LaCoRu_{0.05}$-R and $LaCoRu_{0.2}$-R, forming carbonated/hydroxylated species [32,33].

3.3 Catalytic Performance

The selectivity toward hydrogen and the diesel conversion versus time on stream over catalysts derived from the reduction of $LaCoO_3$, $LaCo_{0.95}Ru_{0.05}O_3$ and $LaCo_{0.8}Ru_{0.2}O_3$ are shown in Fig. 9. For all the catalysts, activity-time curves display data scattering that is normal of this type of reaction and arises from a non homogeneous mixture of the reactants [34]. The initial activity indicates that the substitution of cobalt by ruthenium has a favorable effect on the capacity to extract hydrogen from the hydrocarbon molecules contained in diesel fuel, providing more active and stable catalysts. It is observed that all the catalysts suffer a substantial deactivation after 24 hours of reaction, which is favoured by the relatively low reaction temperature, with enhanced coke formation [35] and S poisoning [36,37]. Average values for diesel conversion, 88, 85 and 92% for catalysts derived from $LaCoO_3$, $LaCo_{0.95}Ru_{0.05}O_3$ and $LaCo_{0.8}Ru_{0.2}O_3$, respectively, were obtained although higher and more stable hydrogen yields are found for catalysts with Ru. Thus, the average of the moles of hydrogen and CO produced for each C-atom in the feed are 0.91, 0.99 and 1.35 for catalysts derived from $LaCoO_3$, $LaCo_{0.95}Ru_{0.05}O_3$ and $LaCo_{0.8}Ru_{0.2}O_3$, respectively. The catalyst derived from $LaCoO_3$, shows a decrease in hydrogen production of around 23%. On the contrary, for the catalysts derived from the perovskites with Ru, this decrease is around 16% and 9% for $LaCoRu_{0.05}$-R and $LaCoRu_{0.2}$-R, respectively. The higher capacity of Ru-containing catalysts to extract hydrogen from diesel molecules is also reflected in

Formatiert: Schriftart: (Standard) Arial, Englisch (USA)

Formatiert: Schriftart: (Standard) Arial, Englisch (USA)

Formatiert: Schriftart: (Standard)

Formatiert: Schriftart: (Standard) Arial, Englisch (USA)

Formatiert: Schriftart: (Standard) Arial, Englisch (USA)

Formatiert: Schriftart: (Standard)

the lower proportion of non-reformed hydrocarbons (CH_4, C_2H_4, C_2H_6 and C_3H_6) in the products (Fig. 9).

It can also be observed that the decrease in hydrogen yield is accompanied by an increase in CO for the catalyst derived from $LaCoO_3$ and also, although in a minor way, in the catalyst derived from $LaCo_{0.95}Ru_{0.05}O_3$. This fact is explained in basis to a greater development of the Boudouard reaction ($CO_2 + C \rightarrow 2CO$), favoured, as it will be pointed out in the Discussion, by a greater formation of carbon in above catalysts, which push this reaction forward.

3.4 Characterization of catalysts after reaction

XRD analyses performed on catalysts after reaction (Fig. 10) show the presence of $La_2O_2CO_3$ (JCPDS 37-804), Co^0 (JCPDS 15-806) and graphitic carbon (JCPDS 75-1621). As in the case of the fresh reduced catalysts, none of the used catalysts exhibited any reflection corresponding to metallic ruthenium and a lower intensity carbon diffraction peak is observed in catalysts derived from Ru-substituted perovskite precursors. Table 4 shows the mean crystallite size of the La and Co phases in the used catalysts calculated by application of the Scherrer equation using the most intense and non-overlapped diffraction peaks (30.2º and 44.0º, respectively). Obtained results highlight that the average particle size of these phases decreases for the catalyst derived from perovskites substituted with Ru.

XPS analysis of the catalysts after reaction was also performed in order to determine the evolution of the surface composition under reaction conditions. Although it is not presented, Co 2p, La 3d and C 1s spectra obtained for catalysts after reaction show that the surface of the three systems is mainly composed of lanthanum oxycarbonate, metallic cobalt and graphitic carbon. From XPS spectra, the atomic surface ratios of the used catalysts have been calculated and the results are shown in Table 4. The used catalysts containing Ru showed a greater ratio (Co+Ru)/La and also a higher exposition of cobalt phase.

Elemental chemical analyses were performed to quantify the carbonaceous and sulphur residues deposited on the catalysts after the activity tests (Table 5). These results indicated different amount of carbonaceous and sulphur deposits on the used catalysts depending on the presence of ruthenium in the catalyst formulation. After reaction, the Ru-containing catalysts reveal some lowering of sulphur deposition on catalysts and an important decrease in carbon deposits. The decrease in the quantity of carbon deposited was close to 70% for the catalyst derived from $LaCoRu_{0.2}$ with

respect to the catalyst derived from bare $LaCoO_3$. This result is in accordance with the higher activity and stability observed for the catalysts containing Ru in its formulation.

4. Discussion

$LaCoO_3$ and $LaCo_{1-x}Ru_xO_3$ mixed oxides (x = 0.05 and 0.2) have been prepared by sol-gel modified Pechini method. This preparation methodology was chosen amongst others to obtain purer perovskites and the efficiency of the catalyst precursors for hydrogen production from diesel oxidative reforming reactions probed [33].

The physical-chemical characterization of the $LaCo_{1-x}Ru_xO_3$ perovskite precursors pointed out that the partial substitution of Co by Ru, produces changes at textural and structural levels. Characterization of precursors by XRD showed a decrease of more than 50% in crystallite domain size following the substitution of Co by Ru in the perovskite lattice (Table 1). The partial substitution of Co also leads to textural changes of the perovskites. The textural characterization of perovskite precursors showed a macro-porous texture for all samples with an increase in the surface area with the substitution of Co by Ru (Table 1). Since the perovskites do not present internal porosity, this result is explained from an increase in the geometrical external area of perovskite particles.

Structural characterization of perovskite precursors by XRD (Figure 2) indicated the distortion of the rhombohedral structure of bare $LaCoO_3$ when cobalt is substituted by ruthenium. The shift of diffraction lines toward lower values indicates the insertion of ruthenium cations into the B position in the perovskite lattice. Considering that calcination during the final step of the syntheses of the perovskites is carried out in air, it is assumed that most of ruthenium is introduced as Ru^{4+} [13~~13~~-15~~15~~].

The difference in the characteristics of the perovskite precursors affects the structure and morphology of the derived catalysts formed after the thermal reduction of the precursors. In-situ XRD measurements under a reductive atmosphere shows the modifications produced in the structure of the perovskites under the activation performed prior to the activity tests. All the perovskites suffer a deep structural transformation toward systems constituted by Co^0 and Ru^0 particles over a matrix of lanthanum oxide. It is observed that the perovskites suffer a reduction process through the formation of different structures with Co^{2+}, such as La and Co spinel oxide (La_2CoO_4) and some structures corresponding to Ruddlesden-Popper series ($La_{m+1}Co_mO_{3m+1}$) such as $La_4Co_3O_{10}$. The appearance of these new phases is observed at 673 K for bare $LaCoO_3$. The comparison of the diffraction patterns during the

Formatiert: Schriftart: (Standard) Arial, Englisch (USA)

Formatiert: Schriftart: (Standard) Arial, Englisch (USA)

reduction of the different perovskites provides some insights about how the presence of Ru in the structure affects the reducibility.

For the perovskites with Ru, the appearance of those phases containing Co^{2+} and Co^0, takes place at temperatures substantially lower, that those observed in the case of bare $LaCoO_3$. This fact is in accordance with the shift of the reduction peaks toward lower temperatures observed in the reduction profile of Ru-containing perovskites (Fig. 4). Thus, the presence of Ru in the lattice of the perovskite facilitates the reduction of the perovskite at lower temperatures, which has also been observed when other noble metals, i.e. Pd, are incorporated in the lattice of $LaCoO_3$ [1717]. The catalysts obtained after reduction of perovskites are structurally composed of Co^0 (for catalyst derived from $LaCoO_3$) or Co^0-Ru^0 (for catalysts derived from $LaCo_{1-x}Ru_xO_3$ perovskites over a matrix of La_2O_3, as shown by XRD and TEM (Fig. 3, 5 and 6). Similar values for both mean crystallite size calculated by means of the Scherrer' equation from XRD patterns (table 2) and particle size of metallic cobalt particles, observed by TEM (figures 5 and 6), are found. This result may be related to the smaller size of crystallites found in the original Ru-containing perovskite precursors (Table 1).

Formatiert: Schriftart: (Standard) Arial, Englisch (USA)

The improved reducibility of the perovskite with the presence of Ru in the lattice also has a consequence for the surface composition of the catalysts obtained after thermal reduction of perovskites. Surface analysis by XPS of the reduced catalysts showed a greater reduction degree of cobalt phase in catalysts derived from the perovskites containing Ru (Fig. 8). Moreover, the higher proportion of non-lattice oxygen, associated to carbonated or hydroxylated lanthana, also highlighted the greater reduction degree achieved with the incorporation of Ru in the precursors.

Results derived from activity tests point out a very high conversion of diesel and high hydrogen yields for all the catalysts studied (figure 9). However, catalysts showed differences in initial activity and stability with time on stream. The initial activity values in Fig. 9 indicate that the substitution of cobalt by ruthenium has a favorable effect in the capacity to extract hydrogen from the hydrocarbon molecules contained in diesel fuel. In a general way, the activities of the Co (and Ru) based catalysts are directly related with its surface concentration and interaction of metallic Co (and Ru) particles over the lanthanum oxide surface. Therefore, the order of activity during the first hours of reaction could be explained by the higher exposition of Co and Ru active phases (Table 4) and the higher proportion of metallic cobalt (Fig. 8) achieved in the catalysts derived from the perovskites containing Ru.

Although all the catalysts suffer deactivation with time on stream, higher stability was observed in the catalysts containing Ru (Fig 9). Besides cobalt surface concentration, catalyst deactivation by coking or sulphur were other factors to be considered for describing the evolution of catalytic activity with time on stream. Different quantities of carbonaceous deposits on the used catalysts were detected in the order: $LaCoO_3$-U> $LaCoRu_{0.05}O_3$-U > $LaCoRu_{0.2}O_3$-U (Table 5). Therefore, the higher stability observed for the catalysts with Ru is explained by the higher surface exposure of active phases (Table 4) and the greater contact with lanthanum oxycarbonate, which has a role gasifying coke precursors [38]. Moreover, the smaller crystallite size of cobalt particles in used catalysts, derived from $LaCo_{0.95}Ru_{0.5}O_3$ and $LaCo_{0.8}Ru_{0.2}O_3$ should decrease the formation of coke [39] and the poisoning by sulfur compounds present in the feed [40].

Conclusions

Partial substitution of Co by Ru in $LaCoO_3$ perovskite leads to textural and structural modifications that have a positive influence in the efficiency of derived catalysts to produce hydrogen by oxidative reforming of diesel fuel. $LaCo_{1-x}Ru_xO_3$ (x = 0.05 and 0.2) perovskites, prepared by Pechini sol-gel method, present high crystallinity and purity. The modifications of diffraction patterns with the content of Ru indicate that most of Ru cations are incorporated in the perovskite lattice, producing a distortion of the rhombohedral phase, a decrease in crystal domain and some increase in surface area.

The evolution of the precursors under a reductive heat treatment, studied by in-situ XRD, clearly show that Ru favours the reduction of the perovskite, with the final reduction phases (Co^0 and La_2O_3) appearing at lower temperature and presenting smaller crystallite sizes. The Co^0 and La_2O_3 phases, as well as Ru^0, have been also observed by HRTEM in reduced systems, forming nanometric particles. The better reducibility of perovskite precursors promoted by Ru, has also an effect at the surface level in activated samples, where a decrease in the oxidation state of surface Co with Ru content is found.

The substitution of Co by Ru in the perovskite lattice modifies the behavior of the derived catalysts in the oxidative reforming of diesel, being found to improve the initial activity and stability of the catalysts in perovskites containing Ru. This improvement was related to the higher exposure of metallic active phases (Co and Ru) under reaction and to the formation of smaller crystallites of Co^0 and $La_2O_2CO_3$, from the

reduction of the Ru-containing perovskites that makes the catalysts less prone to deactivation by coke and sulphur deposits.

Acknowledgements

We are grateful to our research sponsors, CAM (P2009/ENE-1743), INTA and King Saud University, (Riyadh, Saudi Arabia). NMT would also like to acknowledge financial support from the JAE-CSIC grant program. In-situ XRD and HRTEM analyses were carried out while MCAG was a visiting research fellow at Queen´s University Belfast and Fritz Haber Institute, respectively. She would like to acknowledge both groups for their hospitality and for the financial support to access the CenTACat (Centre for the Theory and Application of Catalysis) facilities through EU funded FP6 "Structuring the European Research Area" Program and to DFG (Deutsche Forschungsgemeinschaft, German Research Foundation) and CSIC (Consejo Superior de Investigaciones Científicas). We thank Joana M. Frontela (CEPSA R&D Laboratory, Madrid) for kindly supplying the diesel used in the activity tests.

References

1. R.M. Navarro, M.C. Álvarez-Galván, J.A. Villoria, I.D. González, F. Rosa, J.L.G. Fierro, Appl. Catal. B: Environ. 73 (2007), 247-258
2. K. Kochloefl, Steam reforming. In: G. Ertl, H. Knözinger and J. Weitkamp, Editors, Handbook of Heterogeneous Catalysis vol. 4, Viley VCH, Weinheim (1997), pp. 1819–1831
3. J.R. Rostrup-Nielsen, Phys. Chem. Chem. Phys. 3 (2001) 283–288
4. A.F. Ghenciu, Curr. Op. Solid State Mat. Sci. 6 (2002) 389-399
5. C.H. Bartholomew, Catal. Rev.-Sci. Eng. 24 (1982) 67
6. T. Nakamura, G. Petzow, L.J. Gauckler, Mater. Res. Bull. 14 (1979) 649.
7. J.R. Mawdsley, T.R. Krause, Appl. Catal. A: Gen. 334 (2008) 311-320
8. M.A. Peña, J.L.G. Fierro, Chem. Rev., 101 (2001) 1981-2017
9. N. Mota, M.C. Álvarez-Galván, J.A. Villoria, F. Rosa, J.L.G. Fierro, R.M. Navarro, Topics Catal. 52 (2009) 1995-2000
10. N. Mota, R.M. Navarro, M.C. Álvarez-Galván, S.M. Al-Zahrani, J..L.G. Fierro, J. Power Sources, in press
11. M.P. Pechini, United States Patent Office, 3, 330, 673 (1967)

12. C.D. Wagner, L.E. Davis, M.V. Zeller, J.A. Taylor, R.H. Raymond, L.H. Gale, Surface Interface Anal. 3 (1981) 211-225
13. N. Labhsetwar, P. Doggali, P. Chankapure, D. Valechha, S. Lokhande, A. Watanabe, S. Rayalu, H. Haneda, T. Mitsuhashi, Top. Catal. 52 (2009) 1909-1914
14. N.K. Labhsetwa, M. Dhakad, S.S. Rayalu, R. Kumar, J. Subrt, H. Haneda, S. Devotta, T. Mitsuhashi, Top. Catal. 42-43 (2007) 299-302
15. N.K. Labhsetwar, A. Watanabe, T. Mitsuhashi, Appl. Catal. B. Environ. 40 (2003) 21-30
16. E. Pietri, A. Barrios, O. Gonzalez, M.R. Goldwasser, M.J. Pérez-Zurita, M.L. Cubeiro, J. Goldwasser, L. Leclercq, G. Leclercq, L. Gengembre, Stud. Surf. Sci. Catal. (2001) 136 (2001) 381-386
17. G.L. Chiarello, J.D. Grunwaldt, D. Ferri, F. Krumeich, C. Oliva, L. Forni, A. Baiker, J. Catal. 252 (2007) 127-136
18. S. Ivanova, A. Senyshyn, E. Zhecheva, K. Tenchev, V. Nikolov, R. Stoyanova, H. Fuess, J. Alloys Comp. 480 (2009) 279
19. T. Nakamura. G. Petzov, L.J. Gauckler, Mater. Res. Bull. 14 (1979) 649
20. M. Crespin, W.K. Hall, J. Catal. 69 (1981) 359
21. Szabo, M. Bassir, A. van Neste, S. Kaliaguine, Appl. Catal. B: Environ. 37 (2002) 175-
22. L. Huang, M. Bassir, S. Kaliaguine, Appl. Surf. Sci. 243 (2005) 360.
23. H.F.J. van`t Blik, D.C. Koningsberger, R. Prins, J. Catal. 97 (1986)
24. In: E. J. Mittemeijer, P. Scardi, editors. Diffraction analysis of the microstructure of material, Eds., Springer, Berlin, 2004
25. In: J.R. Davis, Editor, ASM specialty handbook, Nickel, Cobalt, and their alloys, ASM International, Materials Park, OH, US, 2000.
26. H.A.E. Hagelin-Weaver, G.B. Hoflund, D.M. Minahan, G.N. Salaita, Appl. Surf. Sci. 235 (2004) 420-448
27. M.C. Álvarez-Galván, D.A. Constantinou, R.M. Navarro, J.A. Villoria, J.L.G. Fierro, A.M. Efstathiou, Appl. Catal. B: Environ. 102 (2011) 291-301
28. E. Bontempi, L. Armelao, D. Barreca, L. Bertolo, G. Bottaro, E. Pierangelo, L.E. Depero, Crystal Eng. 5 (2002) 291-298
29. L.G. Tejuca, J.L.G. Fierro, J.M.D. Tascón, Adv. Catal. 36 (1989) 237
30. M. M. Natile, E. Ugel, C. Maccato, A. Glisenti, *Applied Catalysis B-Environmental* 72 (2007) 351-362
31. P. Fleming,, R.A. Farrell, R. A., J.D. Holmes, M.A. Morris, J. Am. Ceram. Soc. 93 (2010) 1187-1194

32. E. A. Lombardo, K. Tanaka, I. Toyoshima. J. Catal. 80 (1983) 340-349
33. J.A. Villoria, M.C. Alvarez-Galvan, S.M. Al-Zahrani, P. Palmisano, S. Specchia, V. Specchia, J.L.G. Fierro, R.M. Navarro, Appl. Catal. B. Environ. (in press)
34. S. Yoon, I. Kang, J. Bae, Int. J. Hydrogen Energy 34 (2009) 1844-1851
35. D.L. Trimm, Appl. Catal, 5 (1983) 263-290
36. R.M. Navarro, M.A. Peña, J.L.G. Fierro, Chem. Rev. 107 (2007) 3952-3991
37. C. Palm, P. Cremer, R. Peters, D. Stolten. J. Power Sources 106 (2002) 231-237
38. A.N. Fatsikostas, D.I. Kondarides, X.E. Verykios, Catal. Today, 75 (2002) 145-155
39. J.R. Rostrup-Nielsen, Catal. Today 63 (2000) 159-164
40. A. Borgna, T.F. Garetto, A. Monzon, J. Chem. Soc. Faraday Trans. 93 (1997) 2445

Figure captions

Figure 1. XRD patterns of $LaCo_{1-x}Ru_xO_3$ (precursors of catalysts) (x = 0, 0.05, 0.2) (R. $LaCoO_3$ rhombohedral, C. Co_3O_4 cubic)

Figure 2. XRD detail of $LaCo_{1-x}Ru_xO_3$ (x = 0, 0.05, 0.2) precursors in the region 28-44º and 31-35º (R. $LaCoO_3$ rhombohedral, C. Co_3O_4 cubic)

Figure 3. XRD patterns and evolution of phases obtained under a reductive heat treatment (10% H_2/N_2) from (A): $LaCoO_3$, (B): $LaCo_{0.95}Ru_{0.05}O_3$, (C): $LaCo_{0.8}Ru_{0.2}O_3$ (●$LaCoO_3$ rhombohedral, ○$LaCoO_3$ rhombohedral, ▼Co_3O_4 cubic, ■La_2O_3 hexagonal, ▫La_2O_3 cubic, ▲Co^0 cubic)

Figure 4. TPR profiles of $LaCo_{1-x}Ru_xO_3$ (x = 0, 0.05, 0.2) precursors

Figure 5. Typical HR-TEM image of catalyst derived from the reduction of bare $LaCoO_3$ precursor

Figure 6. Typical HR-TEM image of catalyst derived from the reduction of $LaCo_{0.8}Ru_{0.2}O_3$ precursor

Figure 7. Annular Dark Field (ADF) STEM images and corresponding EDX elemental maps of Co, La and Ru for the catalysts derived from the reduction of $LaCoO_3$ (top) and $LaCo_{0.8}Ru_{0.2}O_3$ (bottom)

Figure 8. Co 2p and La 3d core level XPS of catalysts derived from the reduction of $LaCo_{1-x}Ru_xO_3$ (x = 0, 0.05, 0.2) precursors

Figure 9. Diesel conversion and product distribution during oxidative reforming of diesel over LaCo-R, $LaCoRu_{0.05}$-R and $LaCoRu_{0.2}$-R catalysts (Diesel conversion (%), % H_2, % CO, % CO_2, % CH_4, % C_2H_4, C_2H_6, C_3H_6, 1023 K, 20,000 h^{-1}, 24 h, $H_2O/O_2/C$=3/0.5/1).

Figure 10. XRD patterns of catalysts after reaction, derived from $LaCo_{1-x}Ru_xO_3$ (x = 0, 0.05, 0.2) in the region 20-60º (H. $La_2O_2CO_3$ hexagonal, C. Co^0 cubic, H^. C graphitic hexagonal)

Tables

Table 1. Surface area and average grain size of perovskites $LaCo_{1-x}Ru_xO_3$ (x = 0, 0.05, 0.2) obtained from XRD data

Sample	Surface area (m^2/g)	Average grain size (nm)
$LaCoO_3$	1.1	54
$LaCoRu_{0.05}$	3.1	24
$LaCoRu_{0.2}$	2.9	20

Table 2. Average grain size of different phases after thermal reduction of $LaCo_{1-x}Ru_xO_3$ perovskites and after reaction different phases in fresh and used catalysts derived from $LaCo_{1-x}Ru_xO_3$ perovskites (x = 0, 0.05, 0.2)

Reduced			After reaction		
	La_2O_3 (nm)	Co^0 (nm)		$La_2O_2CO_3$ (nm)	Co (nm)
$LaCoO_3$-R	23	20	$LaCoO_3$-U	33	19
$LaCoRu_{0.05}$-R	18	13	$LaCoRu_{0.05}$-U	30	12
$LaCoRu_{0.2}$-R	17	8	$LaCoRu_{0.2}$-U	29	14

Table 3. Results of EDAX analyses for fresh catalysts derived from $LaCoO_3$ and $LaCo_{0.8}Ru_{0.2}O_3$

% atom	From reduced $LaCoO_3$					Average values
La	56.3	60.3	42.4	39.2	58.6	**51.4**
Co	43.7	39.7	57.6	60.8	41.4	**48.6**
% atom	**From reduced $LaCo_{0.8}Ru_{0.2}O_3$**					**Average values**
La	42.5	56.3	57.7	-	-	**52.2**
Co	50.9	35.8	35.9	-	-	**40.9**
Ru	6.6	7.9	6.4			**7**

Table 4. Surface (XPS) atomic ratios of fresh and used catalysts

	Co/La	Ru/La	(Co+Ru)/La
Fresh reduced catalysts			
$LaCoO_3$-R	0.27 (1)	-	0.27(1)
$LaCoRu_{0.05}$-R	0.28 (1)	0.07 (0.05)	0.35 (1)
$LaCoRu_{0.2}$-R	0.08 (0.8)	0.26 (0.2)	0.33 (1)
Used catalysts			
$LaCoO_3$-U	0.41 (1)	-	0.41 (1)
$LaCoRu_{0.05}$-U	1.34 (0.95)	0.18 (0.05)	1.52 (1)
$LaCoRu_{0.2}$-U	0.56 (0.8)	0.34 (0.2)	0.90 (1)

Nominal values in parentheses

Table 5. Carbon and sulfur content (%) on used catalysts

Used Catalysts	% C	% S
$LaCoO_3$-U	8.9	0.05
$LaCoRu_{0.05}$-U	4.3	0.03
$LaCoRu_{0.2}$-U	2.4	0.03

Figures

Figure 1

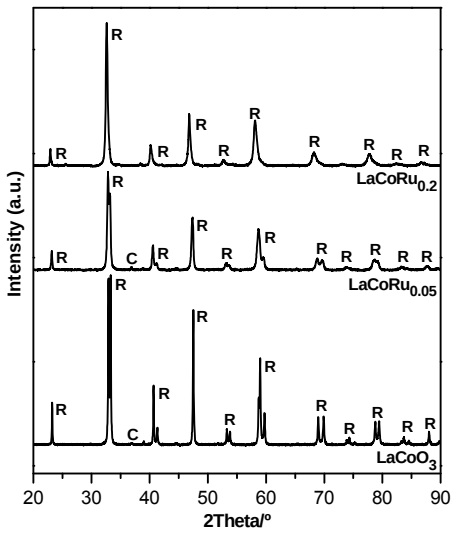

Figure 2

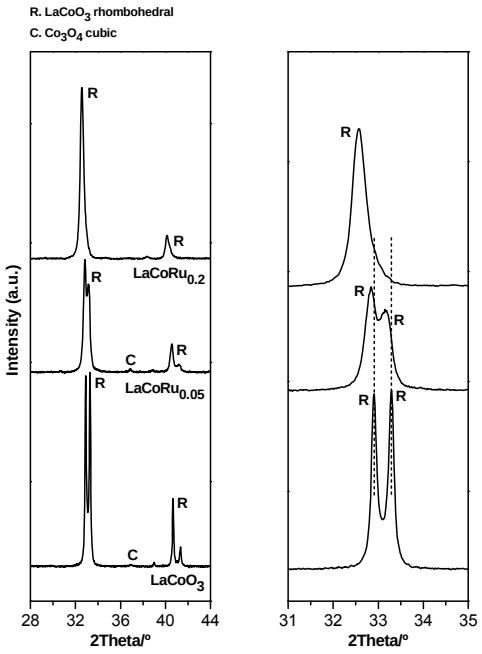
R. LaCoO3 rhombohedral
C. Co3O4 cubic
Intensity (a.u.)
LaCoRu0.2
LaCoRu0.05
LaCoO3
R
C
28
32
36
40
44
2Theta/°
31
32
33
34
35
2Theta/°

Figure 3

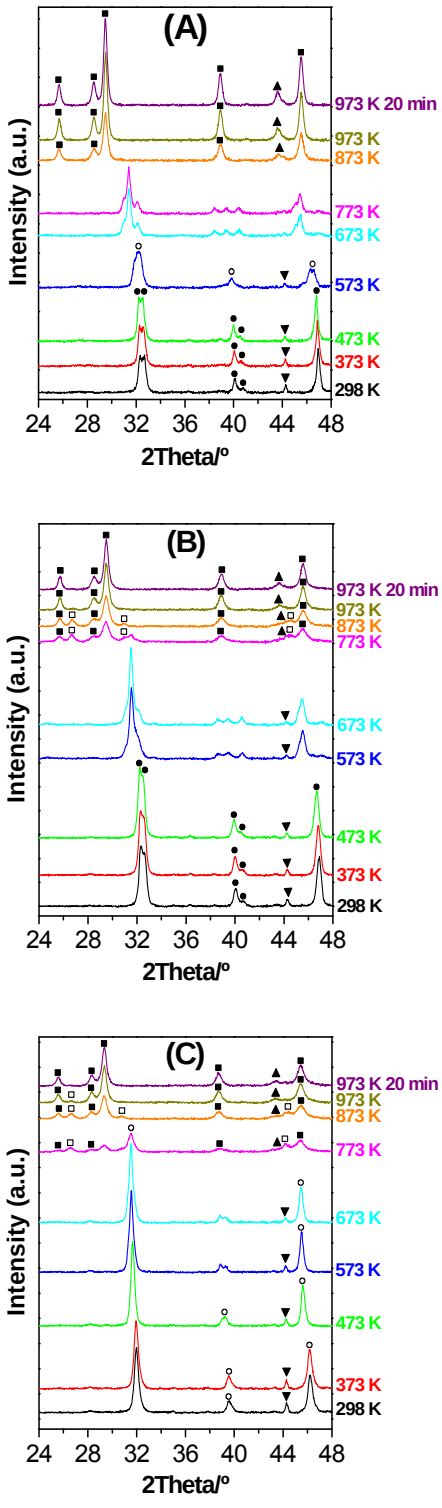
(A)
973 K 20 min
973 K
873 K
773 K
673 K
573 K
473 K
373 K
298 K
Intensity (a.u.)
24 28 32 36 40 44 48
2Theta/º
(B)
973 K 20 min
973 K
873 K
773 K
673 K
573 K
473 K
373 K
298 K
Intensity (a.u.)
24 28 32 36 40 44 48
2Theta/º
(C)
973 K 20 min
973 K
873 K
773 K
673 K
573 K
473 K
373 K
298 K
Intensity (a.u.)
24 28 32 36 40 44 48
2Theta/º

Figure 4

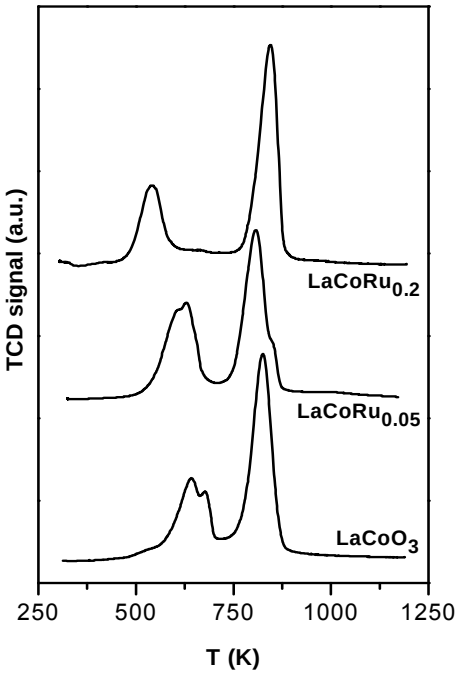
TCD signal (a.u.)
LaCoRu0.2
LaCoRu0.05
LaCoO3
250
500
750
1000
1250
T (K)

Figure 5

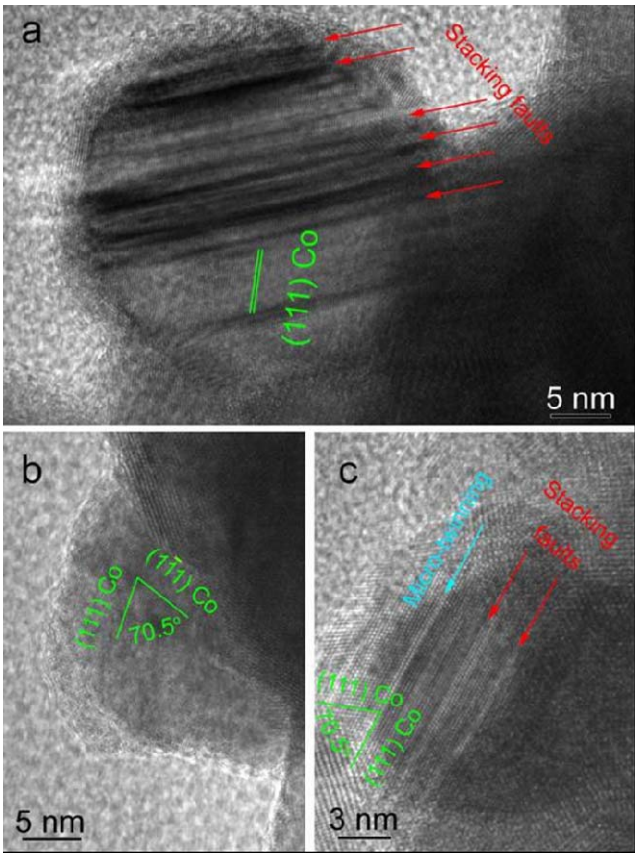
a
Stacking faults
(111) Co
5 nm
b
(111) Co
(1̄11) Co
70.5°
5 nm
c
Stacking faults
(111) Co
(1̄11) Co
70.5°
3 nm

Figure 6

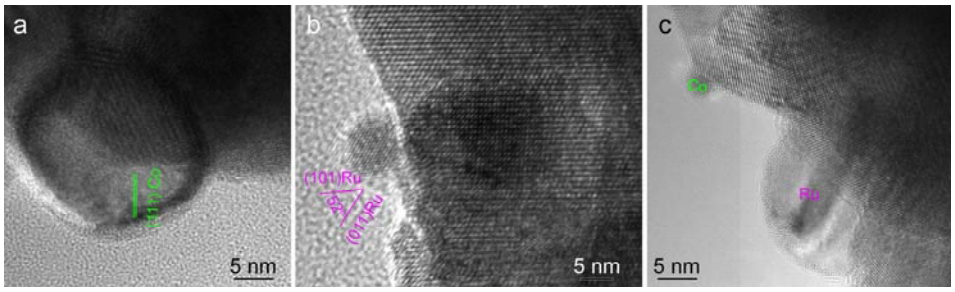

Figure 7

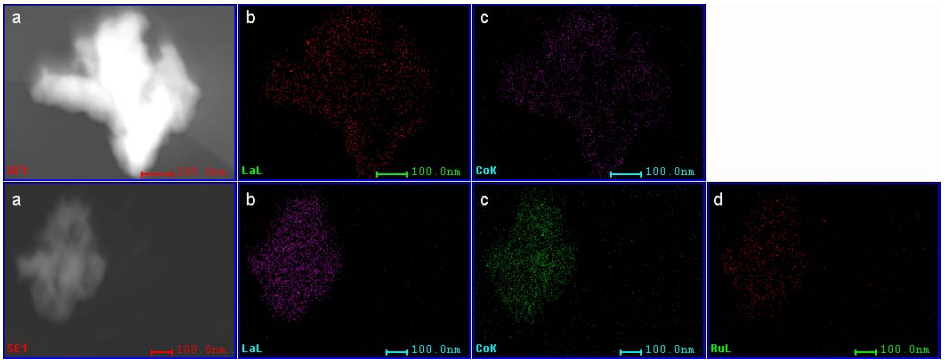

Figure 8

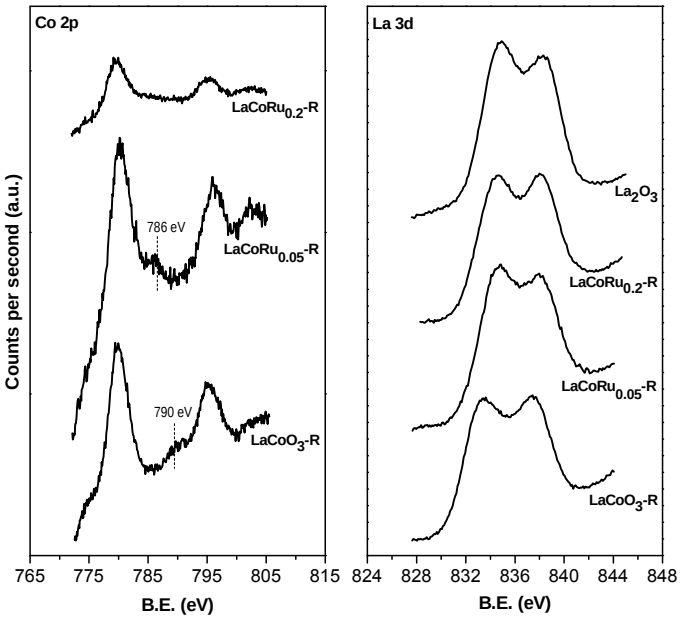
Co 2p
La 3d
Counts per second (a.u.)
LaCoRu0.2-R
786 eV
LaCoRu0.05-R
790 eV
LaCoO3-R
La2O3
LaCoRu0.2-R
LaCoRu0.05-R
LaCoO3-R
765 775 785 795 805 815
824 828 832 836 840 844 848
B.E. (eV)
B.E. (eV)

Figure 9

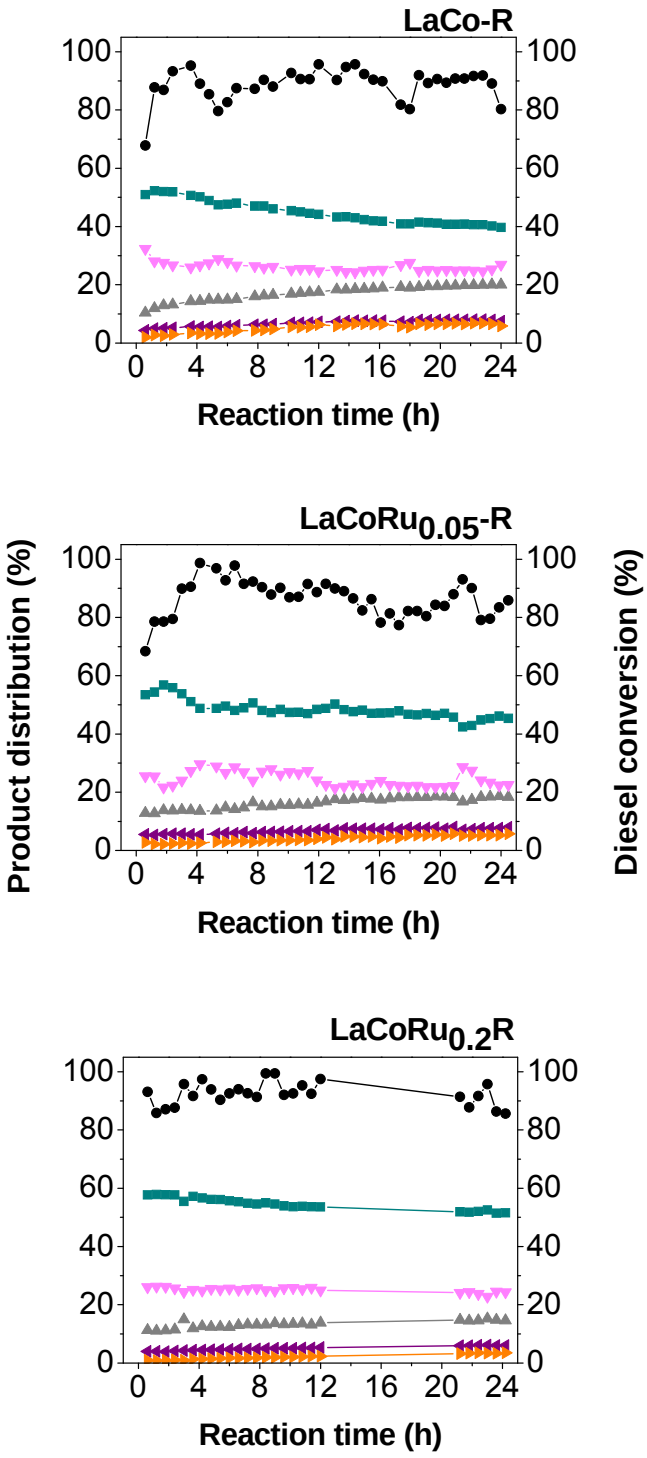
LaCo-R
LaCoRu0.05-R
LaCoRu0.2R
Product distribution (%)
Diesel conversion (%)
Reaction time (h)
0
20
40
60
80
100
0
4
8
12
16
20
24

Figure 10

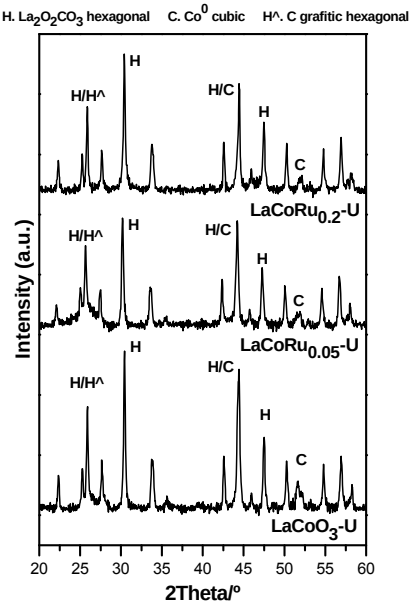
H. La2O2CO3 hexagonal C. Co0 cubic H^. C grafitic hexagonal
Intensity (a.u.)
H
H/H^
H/C
H
C
LaCoRu0.2-U
LaCoRu0.05-U
LaCoO3-U
20 25 30 35 40 45 50 55 60
2Theta/°